**Article:**
Azam, A, Dorgham, A, Morina, A orcid.org/0000-0001-8868-2664 et al. (2 more authors) (2019) A simple deterministic plastoelastohydrodynamic lubrication (PEHL) model in mixed lubrication. Tribology International, 131. pp. 520-529. ISSN 0301-679X

https://doi.org/10.1016/j.triboint.2018.11.011

# A simple deterministic plastoelastohydrodynamic lubrication (PEHL) model in mixed lubrication

Abdullah Azam, Abdel Dorgham, Ardian Morina, Anne Neville, Mark C.T. Wilson

*Institute of Functional Surfaces, School of Mechanical Engineering, University of Leeds, Leeds, UK*

**Abstract**

Most power transmitting components operate under mixed lubrication conditions. Concentrated pressures and smaller lubricant film thickness may cause surface and subsurface stresses to exceed the material yield limit causing permanent geometrical changes. A model was developed to include elastoplastic behaviour within a deterministic unified mixed lubrication framework. Model details are presented and the model is validated against published simulation data. A parametric study to address the effect of material yielding on the contact parameters is performed. It is found that the model successfully produces all the key features of the PEHL contact. The model provides a valuable tool to analyse the PEHL contacts with minimal increase in computational effort and complexity.

*Keywords:* `mixed lubrication, numerical solution, elastic-perfectly plastic, PEHL`

## 1. Introduction

The science of lubrication is the key to the operation and optimization of almost all power transmission components. Rolling element bearings, gear assemblies, cams are a few key examples. Whether oil or grease lubricated, all these components encounter harsh loads and severe environmental conditions. Industry is constantly looking for components that can reliably operate under extreme conditions. This means that the lubricated systems are expected to perform in rather severe conditions. The presence of surface roughness on real engineering surfaces adds another complexity i-e. discrete contact and lubricated spots within the Hertzian contact zone. The resulting lubrication regime is called mixed lubrication. Most lubricated components operate under mixed lubrication conditions. As the load increases, so does the

number of contacts and finally the effect of the lubricant film becomes negligible and the system moves from a state of full film lubrication to boundary lubrication or dry contact conditions. Mixed lubrication models are getting increasingly important.

The mixed lubrication regime links the two extreme conditions of full film regime and the boundary lubrication regime. Thus, a mixed lubrication framework, in essence, converges asymptotically to one of these extremes as the operating conditions change from one extreme to the other. Two distinct mixed lubrication modelling methodologies exist. *Stochastic* models and the *deterministic* models. The *stochastic* models consider the approximate effect of roughness and the film thickness is calculated by the macroscopic geometry of the contact alone. The effects of roughness at the local scale are defined in terms of the statistical parameters which account for the overall effect of roughness. Greenwood and Williamson [1] developed a model for a nominally flat surface in contact against a rough surface. They extended the Hertzian contact theory for single elastic asperity contact to a collection of asperity contacts with Gaussian distribution of asperity heights. The contact model between two nominally flat rough surfaces was given by Greenwood and Tripp [2]. Later, Patir and Cheng [3, 4] proposed the average flow model. They used flow factors to accommodate different roughness patterns and the modified Reynolds equation was solved for a smooth contact condition. Several studies combining the load-compliance criteria from the Greenwood and Tripp [2] model and the average flow model from Patir and Cheng [3] modelled mixed lubrication [5, 6, 7, 8]. The average flow model was later improved by Elrod [9]and Tripp [10] to address the issues arising due to roughness anisotropy. The *stochastic* models provide a convenient tool to analyze the effect of roughness on lubrication characteristics using a limited number of statistical parameters to describe roughness [11]. The limitation of these models was that only the global effect of surface roughness could be analysed. The detailed distribution of pressure peaks, film thickness and deformation within the contact were not accessible. This detailed information is essential in developing an understanding about the lubricant film rupture and the lubrication transition. Thus, with greater availability of computational resources and algorithmic improvements, the trend shifted towards the development of *deterministic* mixed lubrication solvers. These models consider the precise definition of roughness in calculating the gap and film thickness within the contact. Both the macro-geometry and the micro-geometry are used to determine the film thickness. The roughness can be input as single asperity, sinusoidal roughness functions or the true rough surface topography. The challenge then lies in the fact that the problem becomes highly time dependent due to roughness, especially the moving roughness.

Steady state deterministic EHL solutions [12, 13, 14, 15] to the point contact problem started to appear in the late 1980s. These studies assumed that the rough surface was stationary while the smooth counterpart was moving. In reality the rough surface is moving and thus, a transient solution is required. Transient deterministic EHL solvers were presented for a line contact by Ai et al. [16] and for a point contact by Ai and Cheng [17] and Venner and Lubrecht [18] for simplified roughness and by Xu and Sadeghi [19] and Zhu and Ai [20] for real measured roughness.

The *deterministic* mixed lubrication solvers can be further categorized as either *separate* approaches or *unified* approaches. In the *separate* approach, different equations are solved for the solid and lubricated regions. The handling of the transient boundaries between the solid and fluid regions is the key challenge in these models. Jiang et. al. [21] presented the first mixed lubrication model using the separate approach. Later, Zhao et al. [22] used the separate appraoch. The *unified* approach relies in getting both the solid and fluid pressures through the solution of the Reynolds equation. This approach is based upon the idea that under extreme conditions, the pressure flow terms in the Reynolds equation lose their significance. Thus, the entrainment flow terms are also included in building the coefficient matrix. This ensures diagonal dominance under all conditions of operation. The unified approach was first presented by Hu and Zhu [11] and later improved to consider the effect of differential scheme and mesh density [23], the treatment of roughness derivatives [24], the effect of viscosity model [25], the agreement of the model output with the dry contact results [26], effect of finite geometry [27] and the ability to handle arbitrary entrainment speeds [28]. Later, Holmes et al. [29] used the unified approach to develop a mixed lubrication solver based upon the differential deflection method. Li and Kahraman [30] developed a mesh independent unified model by using the asymmetric integrated control volume approach.

The traditional approach to solving the EHL as well as mixed lubrication problems considers only elastic deformation behaviour. In reality, it is often unavoidable to have a system without plastic deformation. The demand for higher power density and high efficiency compact designs is creating a constant challenge for the engineering and research community to design interfaces that can handle extreme conditions. The wind turbines are nowadays designed with power ratings in several megawatts, putting extreme loads on power transmitting components. In some modern power transmission equipments like the continuously variable transmissions, the Hertzian pressure may reach as high as 5 GPa [31]. These pressures are sufficient to cause plastic deformation of the surfaces due to material yield which may in turn modify the lubrication and contact characteristics significantly. Mixed lubrication

models that consider ideally elastic behaviour are prone to producing unrealistically high pressure peaks especially under rough surface conditions. Under such high pressures, the subsurface stress might become several times higher than the material yield limit [32]. The specific case of running in of engineering surfaces is a plastic deformation dominated process. Moreover, the start-stop of any tribological contact inevitably faces mixed lubrication conditions and severe contact conditions due to low speeds where PEHL conditions might prevail.

A good design should ensure that the plastic deformation is kept under control [31] as the reliability of contacting bodies is significantly affected by the presence of plastic deformation [33]. The plastic deformation will cause permanent change on the surfaces affecting both the macro and micro geometry at the contacting interface. Work hardening may also result and eventually, the lubrication and contact characteristics change. Simple EHL solutions will give misleading information under such extreme conditions and accurate information about the film formation and breakdown cannot be obtained. Thus, for a realistic EHL model, plastic deformation should be included. This paper addresses this need for an efficient EHL and mixed lubrication model incorporating plastic deformation.

Several approaches are available for performing rough surface contact simulations [34] and various statistical asperity contact models have been proposed in the past. The pioneering work of Greenwood and Williamson [1] formulated the problem of nominally flat rough surfaces with a statistical representation of asperities. The Hertzian single asperity contact theory was extended to the contact of nominally flat surfaces with statistical distribution of asperities. A recent review summarizes key work in the area of elastic-plastic contact analysis [35]. A rough surface contact model that includes the Johnson, Kendall and Roberts' (JKR) [36] adhesive contact model was presented by Fuller and Tabor [37]. Later, the CEB (Chang-Etsion-Bogy) [38] asperity contact model was presented to account for the elastic-plastic adhesive contact of asperities. This model enjoyed widespread use but was limited due to not being able to handle the discontinuities in the intermediate state of deformation. Zhao et al. [39] presented the ZMC (Zhao-Maietta-Chang) asperity contact model that smoothly links the elastic and plastic deformation through analytical functions. The ZMC model was based upon mathematical manipulations rather than physical understanding [40]. Recent studies by Kogut and Etsion [41] utilized finite element simulations of a single asperity in contact against a flat surface. Their work resulted in empirical expressions to relate different deformation conditions. Their model is called the KE (Kogut-Etsion) model. The elasto-plastic deformation was divided into two empirical equations representing different behaviours of the evolution of

the plastic core below the contact region. They utilized statistical analysis to extend the single asperity deformation to rough surface calculations [42]. Later, the JG (Jackson-Green) [43, 44] model was presented. It was based upon finite element analysis and considered finer meshes and the effect of material properties and geometry. They suggested that the elastic assumption can be valid until the contact interference value of 1.9 times the critical interference value. They also considered the variation of hardness which was considered absent in the KE model. The JG model also concluded that the average pressure to yield strength ratio never reaches 2.8 as suggested by the KE model. The work from Jackson and Green [43] resulted in the following equations that relate the contact parameters for a circular contact to the initial yielding. To derive these equations, the von Mises yield criterion was used which can equally be applied to flattening as well as indentation cases [45].

$$P_y = 1.295e^{0.736\nu\sigma_y} \tag{1}$$

$$W_y = \frac{\pi^3 R^2 p_y^3}{6E^2} \tag{2}$$

$$a_y = \left(\frac{3W_y R}{4E}\right)^{1/3} \tag{3}$$

The critical load, $W_y$ and the critical pressure, $P_y$ are the load and pressure at which initial yielding starts while the critical Hertzian contact radius, $a_y$ is the half width of Hertzian contact corresponding to the initial yield. Here R is the effective radius of curvature at the contact, $\frac{1}{R} = \frac{1}{R_1} + \frac{1}{R_2}$ where $R_1$ and $R_2$ correspond to the radius of curvature of the two bodies, respectively. E is the Young's modulus, $\nu$ is the Poisson's ratio, and $\sigma_y$ is the yield strength of material. To facilitate the discussion and comparison against published results, these parameters will be used throughout the paper.

Only a few attempts have been made until now to include the elastoplastic behaviour into EHL and mixed lubrication models [46]. A 2-D line contact model to study the effect of debris induced indentation was given by Xu et al. [47]. The deformation due to plastic deformation to update topography was calculated using the FEM package and then EHL calculations were run to get new pressures. Niu and Huang [48] gave a line contact EHL model to study elastic-plastic deformation of rough surfaces. They used an elastic-plastic modulus instead of Young's (simple elastic) modulus. A series of studies were conducted more recently by Ren. et al. [31, 49] and He et al. [46, 32] to include plasticity and work hardening into the unified mixed lubrication framework. The volume integration method of Jacq et al. [50]

and Chen et al. [51] to model plastic deformation was used. This model was implemented, first to study the elastoplastic deformation of smooth surfaces and then included simple geometries like a single asperity and single dent. Studies involving sinusoidal and real machined roughness were presented later [49].

This study develops a model to include elasto-plastic behaviour into lubrication analysis. A simplified approach to include elastic-perfectly plastic behaviour in mixed lubricated contact is formulated. The model is then applied to investigate the plastic deformation of a smooth contact which based upon input conditions may be under full film or mixed lubrication conditions. The model provides a convenient way to include plasticity into traditional EHL solvers. The elastic-perfectly plastic model is integrated into a unified mixed lubrication solver and thus requires no distinction as to whether a particular node under load is fluid lubricated or a solid contact spot, also if the plastic deformation is caused by fluid or solid contact pressures, enabling a true PEHL model. Moreover, the algorithm offers several advantages. Minimal modifications to the original EHL solution algorithm are required and compared to the approach of Sahlin et al. [52], this new algorithm requires fewer constraints and can handle plastic deformation due to lubricant pressures as well.

First, the mathematical model is presented with emphasis on the numerical implementation. Then results from the current study are validated against the PEHL simulation results [31], and good agreement is found among the film thickness and pressure profiles. The selection of plastic flow pressure in the current model is critical and detailed discussion on the choice of this parameter is presented. The model exhibits all the key PEHL characteristics. The current study presents the details of the model, initially using smooth surfaces to enable comparison with previous work. The final section then gives an illustration of the application of the PEHL model to rough surfaces.

## 2. Basic PEHL equation set

The EHL equation set contains the Reynolds equation, the film thickness equation and the load balance equation along with the two equations of state relating the density and viscosity of the lubricant to pressure. The same equation set is applied to develop the PEHL model. First of all a mixed lubrication model is developed and then the PEHL model is applied. The mixed lubrication model developed in this work is based upon the semi-system approach [53] which requires the coefficient matrix for solving the Reynolds equation to contain terms from both the pressure flow and the entrainment flow parts of the Reynolds equation. This is to ensure that under

extreme conditions when the pressure flow terms become insignificant, the diagonal dominance is maintained. The coefficient matrix built solely from the pressure flow terms is prone to slow or no convergence especially at higher loads or when high frequency roughness is involved. Hu and Zhu [11] suggest that the pressure flow terms should be turned off when the lubricant film thickness reduces to very small value. Their approach enables the solution of the EHL mixed lubrication problem in a unified manner where both the lubricant and solid contact pressures are calculated by solving the Reynolds equation. When modelling rough surfaces, the flow obstructions arising from asperity contacts manifest themselves in the form of a very small local film thickness. At nodes where the film thickness falls below a certain predefined value (1 nm in this study), the reduction of the pressure flow terms in the Reynolds equation to negligible values represent obstructions to the flow. In the current study, the unified solution algorithm was used. The Reynolds solver based upon the semi-system and the unified algorithm is robust enough to generate lubricant and solid pressures in a single framework. The plastic deformation algorithm will be described in the next sections while a brief summary of the equations describing the EHL and mixed lubrication system is presented in the current section.

The complete pressure profile is computed by solving the Reynolds equation, given as

$$\frac{\partial}{\partial x}\left[\left(\frac{\rho h^3}{12\eta}\right)\frac{\partial p}{\partial x}\right]+\frac{\partial}{\partial y}\left[\left(\frac{\rho h^3}{12\eta}\right)\frac{\partial p}{\partial y}\right]=\left(\frac{u_1+u_2}{2}\right)\frac{\partial(\rho h)}{\partial x}+\frac{\partial(\rho h)}{\partial t} \tag{4}$$

The variables $h$, $\rho$ and $\eta$ define the lubricant film thickness, density and viscosity. The pressure, speed of body 1 and speed of body 2 are given by $p$, $u_1$, $u_2$ while $x$, $y$ represent the coordinate directions and $t$ is the time. The lubricant properties are described through its viscosity. In this study the lubricant is assumed Newtonian and the x-coordinate is aligned with the flow direction. Two boundary conditions are applied. At the boundaries of the solution domain, the boundary condition $p = 0$ is applied. The exit of the EHL contact is diverging and the pressure in this region may fall below the vapour pressure and results in fluid cavitation [54]. The boundary condition to handle this phenomenon is called Swift-Steiber boundary condition or the Reynolds exit conditions and enforces the pressure beyond cavitation boundary, $x_e$, to be zero i.e. $\{\forall\ x \geq x_e,\ p < 0 \Rightarrow p = 0\}$.

The film thickness equation for the point contact is expressed by combining all the terms defining the gap between two surfaces.

$$h = h_0(t) + \frac{x^2}{2R_x} + \frac{x^2}{2R_y} + v_e(x, y, t) + \delta(x, y, t) \tag{5}$$

The film thickness is also termed as gap as it defines the relative gap between mating surfaces. In this equation, $h_0(t)$ is the undeformed film thickness. The term $v_e$ describes the total deformation. The deformation may be elastic or elasto-plastic. At this stage the deformation cannot be separated into individual components. The algorithm presented in the next section outlines the procedure for extracting the magnitude of plastic deformation. The variables $R_x$ and $R_y$ define the radius of curvature in the x and y direction respectively while the term $\frac{x^2}{2R_x} + \frac{x^2}{2R_y}$ gives the macro geometry of the contact. The microgeometry is defined deterministically by the roughness term $\delta(x, y, t)$. The surface elastic deformation $v_e$ is represented by the famous Boussinesq integral formulation.

$$v_e = \frac{2}{\pi E'} \int\int_{\sigma} \frac{p(x,y)}{\sqrt{(x'-x)^2 + (y'-y)^2}} dxdy$$

This equation is non-dimensionalised and converted into discrete form and represented as a deformation matrix.

$$V_{ij} = 2\frac{\Delta X}{\pi^2} \sum_{k=1}^{M} \sum_{l=1}^{N} D_{ij}^{kl} P_{kl}$$

In this equation, the matrix $D_{ij}^{kl}$ is called the flexibility matrix and the pressure $P_{kl} = p_{kl}/P_h$, where $P_h$ is the Hertzian pressure. This matrix forms a convolution with pressure which can be solved more efficiently using Fast Fourier Transforms (FFTs). The use of FFTs makes the solution process much quicker and makes denser grids accessible. The deformation matrix is written as a convolution.

$$V(X_i, Y_j) = \sum_{k=1}^{M-1} K(X_i - X_k, Y_j - Y_k) * P(X_k, Y_k)$$

The application of FFTs require the conversion of this linear convolution to a cyclic convolution and the pressure matrix and the flexibility matrix require pre-treatment [55]. The DC-FFT method is computationally much more efficient compared to the other methods for calculation of surface deformation [56]. The viscosity is considered a function of pressure and the Roelands equation is used to describe it.

$$\eta(p) = \exp\left(\ln(\eta_0) + 9.67\right)(-1 + (1 + \frac{P_h}{p_0} p)^z) \tag{6}$$

The term $\eta_0$ is the viscosity at ambient conditions and $z$ is a dimensionless parameter called Roelands pressure viscosity index obtained through curve

fitting. In the current study, z=0.68 was used. The lubricant density is also considered a function of pressure and is calculated using the following equation,

$$\rho = \rho_0 \left( 1 + \frac{0.6X10^{-9}p}{1 + 1.7X10^{-9}p} \right) \tag{7}$$

The load balance equation in the non-dimensionalized form for a point contact is applied as,

$$\sum_{x_i,y_i}^{x_o,y_o} P(X,Y)dXdY = \frac{2\pi}{3} \tag{8}$$

where the $i$ and $o$ values correspond to the inlet and outlet of the solution domain.

These five equations (4 to 8) form a complete set of equations which is solved to get the mixed lubrication pressure and film thickness profiles. The solution requires a robust numerical technique as the equations are highly non-linear in character. An iterative solution process is applied. The pressure at each time step is calculated in an iterative fashion. The pressures are then truncated as described in the next section. The truncated pressures are used to calculate the elasto-plastic deformation. This new deformation then is used to extract the plastic deformation magnitude from the total elasto-plastic deformation. This process is repeated until convergence of film thickness. In the current study, the difference in the film thickness was found to be less than 1 % when the mesh density was changed from 128 x 128 to 256 x 256. Therefore, to be consistent with the work of Ren et al. [31], a mesh of 128 x 128 is employed. Liu et al. [23] also suggest that this mesh density is sufficient to get accurate results.

## 3. Plastic deformation model and algorithm

Plasticity is a non-linear phenomenon and the calculation of plastic deformation is a fairly complex problem. For engineering applications, a simplified approach is required where desired accuracy can be achieved by including assumptions that simplify the problem. This current study is focussed on the engineering applications. The developed model is expected to give conservative estimates about the material failure but the design process can be complimented with suitable factors of safety. Thus, the tool developed in this study is of immense engineering value.

The plastic deformation model developed in this work is based upon the idea that the nodes that deform plastically float on the surface to form a plane as shown in figure 2. The criterion for plastic deformation is assumed to be the condition where the pressure at a node reaches the average yielding

pressure. Once a node is under plastic deformation, the pressure on this node is limited to the yielding pressure. This condition is referred to as *floating* in the current study and it is due to this condition that more nodes start to support load and the contact area increases. The yielding pressure is generally found to be 2.8 times the yield strength [57]. The deformation of the nodes in this way eventually forms a plane. Sahlin et al [52] used similar concept to develop an elastic-perfectly plastic model under mixed lubrication. Their model is based upon the assumption of dry contact which requires the application of complementarity condition and is unable to simulate plastic deformation due to lubricant pressure. Thus, it is not a true PEHL model.

In practice, the contact pressures in rough surface EHL simulations can reach values high enough to cause yielding of material especially under severe contact conditions of high load and low speeds. Therefore, a deterministic mixed lubrication solver based upon the unified solution approach was selected and developed in this study. The unified algorithm can give solid and fluid pressures by solving the Reynolds equation alone without defining the solid and fluid contact regions prehand. Moreover, this solver can be used for simulating the entire transition of lubrication regimes. The mixed lubrication solver is modified to include elastic-perfectly plastic behaviour. So, the PEHL algorithm also inherits this strength of being able to simulate the complete lubrication transition from full film to boundary. In the current paper, the unified solution algorithm is modified and extended to study plastically deforming contacts.

The application of the elasto-plastic deformation algorithm requires modifications to be made to the Reynolds solver. The first change is made within the solver, at the point of application of load balance condition. The points that undergo yielding are considered to float and their role in carrying load is limited to the yielding pressure. This is achieved by limiting the pressure values during the summation in equation 8 to the yielding pressure i.e. $\forall P \geq P_y, P = P_y$ while calculating the undeformed film thickness value, $h_o$ in equation 5. This modifies the film thickness values to account for the elasto-plastic contact behaviour. This process gets repeated as it is a part of the pressure and film thickness convergence loops. No other modification is required inside the Reynolds solver.

Once the pressure and film thickness have converged, the nodal pressures are truncated and the reduced elastic deformation is calculated using these truncated pressures. These new deformation values are then used to get the new values of film thickness. The plastic deformation is evaluated by subtracting this new film thickness for all the plastically deforming nodes from the minimum value of the new film thickness among the elastically deforming nodes. The truncated pressure is then given as initial guess to the

EHL solver and the Reynolds solver is again used to get the new pressure profile and film thickness. In this way, the solution moves from purely elastic to elasto-plastic by repeating this process until a stable solution is reached.

There is no need to apply a plane convergence criteria as was done by Sahlin et al. [52]. This is automatically taken care of as the un-deformed film thickness $h_0(t)$ is converged as part of the EHL solver during the film thickness convergence loop. The resulting algorithm is simple enough for engineering applications and extremely useful for performing lubrication transition studies.

The conceptual definition of plastic deformation needs to be revisited here. It has been discussed in detail by Johnson [57] that the material yielding starts at the subsurface and with further increase in load, the size of this plastically deformed zone increases and it eventually reaches the surface. Thus, two yielding pressures can be identified. The initial yielding pressure and the plastic flow pressure. The initial yielding pressure is the pressure at which the plastic deformation starts to occur and a plastic core is formed within the elastic material. This value cannot be used as the hardness of the material. The hardness of the material is related to the value of pressure at which the plastic deformation moves from the subsurface to the surface of the material. At this condition, the actual material flow starts to occur and the pressure is called the plastic flow pressure.

| | symbol | value | units |
|---|---|---|---|
| Applied load | $F$ | 30 | $N$ |
| Radius of curvature (ball) | $R_1$ | 9.525 | $mm$ |
| Radius of curvature (flat) | $R_2$ | $\infty$ | $mm$ |
| Surface speed (ball) | $U_1$ | 0.5 | $m/s$ |
| Surface speed (flat) | $U_2$ | 0.0 | $m/s$ |
| Young's modulus (ball) | $E_1$ | $\infty$ | $GPa$ |
| Young's modulus (flat) | $E_2$ | 219.78 | $GPa$ |
| Dynamic viscosity | $\eta$ | 0.0112 | $Pa.s$ |
| Pressure-viscosity coefficient | $\alpha$ | 14.94 | $GPa^{-1}$ |
| Yield Strength | $\sigma_Y$ | 500 | $MPa$ |

Table 1: Parameter input symbols, values and units

## 4. Numerical implementation

In this section, the numerical issues are discussed and the details of simulation set up are given. The flow chart in figure 1 gives the general procedure

for the solving the PEHL problem. The steps in the algorithm present the key concepts and the way these were implemented.

1. The first step involves the solution of the mixed lubrication problem with the load at the plastically deforming nodes limited to the plastic yielding values. The simulation starts with the Hertzian pressure profile and moves towards a converged solution. Limiting the pressures to yielding values ensures that the plastically deforming nodes carry load only up to the yielding limit. It is important to note that the pressure values are not truncated at this stage.
2. The converged pressure and film thickness profiles are obtained and the deformation values are recorded in a matrix $V_{e+p}$.
3. The pressures are then truncated and the deformation is again calculated based upon these reduced pressures using Boussinesq formulation in another variable, $V_e^{trun}$. This deformation is then used to calculate the gap (film thickness) profile using equation 5.
4. The deformation $V_{e+p}$ is the elastoplastic deformation and the deformation $V_e^{trun}$ is the elastic deformation obtained that would result if the reduced pressures were present in an equivalent elastic contact. At this stage, the distribution of the nodes, $I_e$ undergoing elastic deformation alone and $I_p$ undergoing elasto-plastic deformation is recorded.
5. In this step, The plastic deformation magnitude is extracted by subtracting the deformation $V_e^{trun}$ for the plastically deforming nodes, $I_p$ from the minimum value of deformation $V_{e+p}$ for the elastically deforming nodes, $I_e$.
6. The nodal plastic deformation magnitude is used to update the geometry by permanently deforming the plastically deformed material and this new geometry is input to the mixed lubrication solver again until the plastic deformation magnitude is zero.

The last step in the procedure is only applied if the evolution of the contact pair is simulated. Otherwise, the truncated pressure profile is input into the next simulation step until the PEHL film thickness obtained after successive iteration steps has converged. It was found that 5 iterations are sufficient to get completely converged plastically deformed geometry and the plastic deformation magnitude while in the first iteration, almost 90 % of the plastic deformation magnitude has already been predicted by the solver. It was also found that irrespective of the number of iterations to reach the final geometry, when the evolution of the contact pair is considered, the final deformed geometry is always the same. In terms of numerical effort, to converge the pressure difference to less than $1 \times 10^{-6}$, a single iteration for

the smallest load of 10 N takes ≈ 16 s for the EHL calculations and ≈ 10 s for a PEHL calculations on a standard single core of the computation. But considering the fact that it takes almost 5 iterations to completely predict the plastic deformation, a single PEHL calculation requires almost 3 times more computational effort.

To illustrate the model output and validity, the contact between a rigid ball and deformable flat is realized. The flat is assumed to be an elastic-perfectly plastic semi-infinite solid. The ball motion is defined by its speed, $U_1 > 0$ and the flat is assumed stationary $U_2 = 0$. At every step, the plastic deformation gets accumulated until plastic deformation itself converges and so does the film thickness.

The input parameters have been summarized in table 1. For all the simulation cases presented in this paper, the material yield strength is considered to be 500 MPa. This corresponds to a critical pressure of 807 MPa and critical load of 5.11 N. The ball diameter is 19.05 mm and ball speed is fixed at $U_1 = 0.5m/s$ which gives an entrainment speed of $U_r = 0.25m/s$. Different load values were used to develop the plots in the following sections. Six different load values were chosen (between 10 N and 125 N) to consider the contact condition from fully elastic to elasto-plastic and finally fully plastic regime. The pressure and film thickness profiles are presented in 2-D at the centre line of the contact along flow direction.

## 5. Model validation and discussion

In this section, the model output is validated against published simulation results [31] and the effect of inclusion of elasto-plastic behaviour on the contact performance is analyzed. Two values of the yielding pressure are used. The initial yielding pressure, using yield strength of 500 MPa comes out to be 0.807 GPa and the plastic flow pressure is taken as $2.22 \times \sigma_y$ and is fixed at 1.110 GPa. A discussion on the choice of the hardness value will be presented at the end of this section.

The simulations were performed by varying the load from 10 N to 125 N in six steps. Figure 3 presents the non-dimensionalized pressure profiles and film thickness profiles for the different load values. The pressure is non-dimensionalized by the yield strength of the material $\sigma_y$ and the film thickness values are non-dimensionalized by the Hertzian contact radius at the initial yielding, $a_y$. The presence of the pressure spike can be clearly seen in the pressure profiles but only for the cases where the yielding pressure is greater than the pressure value at which the pressure spike appears. Otherwise the pressure profile is flattened as soon as it reaches the material yielding limit. The film thickness profile shows flatness at the middle of the contact region

and the exit constriction appears much sharper. It can be seen that with increasing load, the flatness of the profile increases and at the highest load it spans the complete contact region. The exit constriction also gets sharper and deeper with increasing load.

The plastic deformation magnitude and profile are plotted in figure 4. It is to be noted that for the smallest load value used the predicted plastic deformation is zero. The plastic deformation profiles also suggest that the deformation occurs smoothly from the middle to the sides of the contact. Moreover, the contact area is also expected to increase as more and more plastic deformation takes place.

A close comparison of the results presented in figure 3 and the PEHL results presented by Ren et al. [31] shows that the current model produces almost identical pressure profiles. Due to the nature of the model, the reduction of the pressure in the middle region of the contact zone is not observed and a flat pressure profile with pressures capped at the yielding value of 1.110 GPa is present. The overall pressure profiles have been predicted very accurately. The pressure and the area increase predicted by the current model in comparison to the predictions of Ren et al. [31] is presented in figure 5. The pressure predictions match almost exactly but the area increase is under predicted by the current model. This was expected as the current model is a simple version of PEHL.

The film thickness profiles in figure 3,on the other hand, do not match exactly. The overall qualitative trend matches fairly well but quantitative differences exist. It was found that these differences are not only present in the PEHL results but also in the EHL results. The EHL film thickness profiles were digitized from Ren's work [31] and plotted against the film thickness profiles from the current study in figure 6. The current PEHL model predicts consistently thicker lubricant films. Next, the magnitude and trend of the differences in the film thickness values at the centre of the contact were plotted in figure 7. The quantitative differences in the EHL predictions may result due to the differences in the numerical solution procedures and the discretization schemes used to solve the problem. A detailed study addressing the effect of mesh density and discretization schemes in EHL / mixed lubrication solvers was presented by Liu et al. [23]. Once these differences in the EHL predictions are accounted for, the quantitative match among the PEHL film thickness predictions is improved as shown in figure 8. The differences in the central film thickness prediction still exist, albeit greatly reduced but the minimum film thickness values and the point in space where this minimum film thickness occurs match exactly.

The PEHL model presented is based upon defining a hardness value for the material to consider its yielding once the pressure exceeds this hardness

value. It was found that the model output is sensitive to the choice of this hardness value. A sensitivity analysis was performed by varying the hardness value from 800 MPa, slightly below the initial yielding pressure to 1500 MPa. For all these cases, the load was fixed at 75 N and the rest of the parameters were kept the same as given in table 1. The pressure and film thickness profiles were plotted for varying values of hardness and are shown in figure 9. It is observed that as the average yielding pressure is decreased, more and more plastic deformation takes place. Smaller contact areas are observed for higher hardness values. It is also observed that the pressure profiles predicted from the current PEHL model give very good qualitative and quantitative match with the results of Ren et al. [31] at a hardness value of $\approx 2.3 \times \sigma_Y$ while excellent qualitative and quantitative agreement is found between the film thickness predictions from the current model and Ren et al.'s [31] results when the hardness value moves from 2.8 $\times \Sigma_y$ towards $\Sigma_y$. Moreover, if the permanent deformation of material is taken into account by considering the permanently deformed material to be physically not present in successive EHL / mixed lubrication solution iterations, the predictions from the current model improve. Ren et al. [31] also included the work hardening property by assuming a linear variation of stresses with yielding which might be a reason for the slight mismatch of the predictions. These differences are expected considering the simplicity and ease of implementation of the model. Nevertheless, the current model successfully produces all the key features of the PEHL and gives results within reasonable accuracy which are very useful for design purposes.

Hardness is defined as the average pressure in a contact under fully plastic deformation. Jackson and Green [43] simulated the contact between a deformable sphere and a rigid flat using finite element analysis. The increase in deformation of the sphere was found to reduce the average pressure from about 2.84 times the yield strength towards the yield strength value. The average pressure is the same as hardness as used by Tabor [58] and Ishlinskii [59]. Later, Wadwalkar et al. [60] showed that the average pressure / hardness approaches the yield strength as the deformation increases. This is due to the fact that the shape of the sphere changes to a punch with deformation increase [45]. Several equations have been suggested that relates the deformation to the hardness and yield strength of the material [61].

Mesarovic and Fleck [62] analysed indentation of a deformable flat by a rigid sphere. They also found that at large deformations, the average pressure decreases to less than 2.8 times the yield strength. Kogut and Etsion performed elastic-plastic indentation analysis and found that the reduction of the hardness value was similar to the flattening analysis performed by Jackson and Green [43]. Later, Ye and Komvopoulos [63] and Kogut and

Komvopoulos [64] suggested that the indentation pressure in an elastic-plastic contact case was always lower than the popular value of 2.8 times the yield strength [45]. They formulated an equation to relate the change in the average pressure as a function of the ratio of combined elastic modulus to the yield strength. Indentation of spherical metallic surfaces was performed by Alcalá and Esqué-de los [65]. They found that the change in average pressure with deformation was similar to previous observations, in the absence of hardening or pileup. Yu and Blanchard [66] curve fitted data from literature and found a similar relationship between geometry and hardness. Therefore, the fact that the current model gives better match at the magnitude of the hardness value below 2.8 is in line with the findings and suggestions of previous studies. Jackson and Green suggest that the ratio of average pressure to yield strength never reaches 2.8 [43, 44]. The differences among the predictions from the current model against simulation data are greater at higher loads. This may be due to the fact that the geometry changes from a rigid ball on a deformable flat to a rigid punch deforming the flat or in the case of rigid flat and deformable ball, the geometry of the ball changes significantly forming a flat faced object. It has been suggested recently by Jackson et al. [45] that as the ratio of contact area to the radius of curvature moves towards unity (with increasing load), the ratio of hardness to yield strength moves towards unity as well. For an intermediate state, $0 < \frac{a}{R} < 1$, the ratio of hardness to yield strength lies between 2.84 and 1 i.e. $2.84 > \frac{H}{\sigma_y} > 1$. Therefore, the output from the current model deviates at higher loads due to the fact that the hardness is also changing at higher loads. It is expected that due to this variation in hardness, with increase in load values, the film thickness predictions from the current model give better match against Ren et al. [31] if the Hardness to yield strength ratio moves towards unity.

The general behaviour of an elastoplastic contact resembles that of the EHL behaviour. The film thickness profiles retain their typical EHL character. The exit constriction is visible at all load values. It can be seen that due to plasticity, the film thickness profile becomes much flattened at the middle region of the contact and this flatness increases with applied load. The model developed in the current study gives estimate of the PEHL pressure and film thickness profiles within reasonable accuracy and provides a highly valuable tool in the design of lubricating interfaces.

## 6. Application to rough surfaces

The current section illustrates the application of the PEHL model to the elasto-plastic contact of rough surfaces. The real rough surfaces are characterized by randomness and irregular features. The PEHL characteristics

are greatly affected by these features. It is the permanent changes in these features that results in the running in of surfaces. Therefore, there is a growing need to develop the capability of simulating PEHL in contacts involving real machined roughness. The roughness was generated numerically using the method of Hu and Tonder [67]. Figure 10 presents the center line PEHL results for the pressure profiles, film thickness profiles and the original and deformed geometry of the rough ball. The corresponding EHL results are also presented for comparison. The input conditions were kept the same as for smooth surface cases (see table 1) and the load was fixed at 10 N. The ball surface was considered to be elastic perfectly plastic while the flat was assumed to be rigid. A roughness of 35 nm was imposed on the ball surface while the disc was assumed to be smooth. The hardness value was chosen to be $\approx 2.3 \times \sigma_y$ where $\sigma_y = 500$ MPa. The pressure profile shows the flattening of pressure values to the imposed hardness value corresponding to the plastically deforming nodes. The merging of the two pressure peaks at the centre of the contact for the PEHL simulation results in area increase. The film thickness for the PEHL case is reduced at certain nodes. It can be seen that the nodes corresponding to film thickness reduction due to elastoplastic deformation do not coincide with the pressure peaks. On the other hand, the asperities corresponding to the pressure peaks at the centre of contact undergo large flattening. The contact during these simulations was under mixed lubrication conditions with a contact area ratio of 7 %.

## 7. Conclusion

A method to include elastic-perfectly plastic behaviour in the mixed lubrication models was developed and presented. The model algorithm and the implementation details are given. The model successfully produces all the general features of PEHL and was validated against published simulation results. It was found that the model is robust and computationally very efficient requiring minimal changes to the existing EHL solution algorithms and is able to quantify plastic deformation, changes in film thickness and geometry within reasonable accuracy, providing an invaluable tool for engineering applications.

## Acknowledgement

The study was funded by the FP7 program through the Marie Curie Initial Training Network (MC-ITN) entitled "FUTUREBET - Formulating an Understanding of Tribocorrosion in ardUous Real Environments - Bearing

Emerging Technologies" under grand no. 317334 and was carried out at the University of Leeds.

## References


[1] JA Greenwood and JBP Williamson. Contact of nominally flat surfaces. *Proc. R. Soc. Lond. A*, 295(1442):300–319, 1966.

[2] JA Greenwood and JH Tripp. The contact of two nominally flat rough surfaces. *Proceedings of the institution of mechanical engineers*, 185(1):625–633, 1970.

[3] N Patir and HS Cheng. An average flow model for determining effects of three-dimensional roughness on partial hydrodynamic lubrication. *Journal of lubrication Technology*, 100(1):12–17, 1978.

[4] N Patir and HS Cheng. Application of average flow model to lubrication between rough sliding surfaces. *Journal of Lubrication Technology*, 101(2):220–229, 1979.

[5] B C Majumdar and B J Hamrock. Effect of surface roughness on elastohydrodynamic line contact. *Journal of Lubrication Technology*, 104(3):401–407, 1982.

[6] J Prakash and H Czichos. Influence of surface roughness and its orientation on partial elastohydrodynamic lubrication of rollers. *Journal of lubrication technology*, 105(4):591–597, 1983.

[7] D Zhu and HS Cheng. Effect of surface roughness on the point contact ehl. *Journal of tribology*, 110(1):32–37, 1988.

[8] D Zhu, H S Cheng, and B J Hamrock. Effect of surface roughness on pressure spike and film constriction in elastohydrodynamically lubricated line contacts. *Tribology Transactions*, 33(2):267–273, 1990.

[9] H. G. Elrod. A general theory for laminar lubrication with reynolds roughness. *Journal of Tribology*, 101(1):8–14, 1979.

[10] JH Tripp. Surface roughness effects in hydrodynamic lubrication: the flow factor method. *Journal of lubrication technology*, 105(3):458–463, 1983.

[11] Y Z Hu and D Zhu. A full numerical solution to the mixed lubrication in point contacts. *Journal of Tribology*, 122(1):1–9, 2000.

[12] AA Lubrecht, WE Ten Napel, and R Bosma. The influence of longitudinal and transverse roughness on the elastohydrodynamic lubrication of circular contacts. *Journal of tribology*, 110(3):421–426, 1988.

[13] CC Kweh, HP Evans, and RW Snidle. Micro-elastohydrodynamic lubrication of an elliptical contact with transverse and three-dimensional sinusoidal roughness. *Journal of Tribology*, 111(4):577–584, 1989.

[14] C C Kweh, MJ Patching, HP Evans, and RW Snidle. Simulation of elastohydrodynamic contacts between rough surfaces. *Journal of tribology*, 114(3):412–419, 1992.

[15] X Ai and H S Cheng. The effects of surface texture on ehl point contacts. *Transactions of the ASME-F-Journal of Tribology*, 118(1):59–66, 1996.

[16] X Ai, H S Cheng, and L Zheng. A transient model for micro-elastohydrodynamic lubrication with three-dimensional irregularities. *Journal of tribology*, 115(1):102–110, 1993.

[17] X Ai and H S Cheng. The influence of moving dent on point ehl contacts. *Tribology Transactions*, 37(2):323–335, 1994.

[18] C H Venner and AA Lubrecht. Numerical analysis of the influence of waviness on the film thickness of a circular ehl contact. *Journal of tribology*, 118(1):153–161, 1996.

[19] G Xu and F Sadeghi. Thermal ehl analysis of circular contacts with measured surface roughness. *Journal of tribology*, 118(3):473–482, 1996.

[20] D Zhu and X Ai. Point contact ehl based on optically measured three-dimensional rough surfaces. *Journal of tribology*, 119(3):375–384, 1997.

[21] X Jiang, DY Hua, HS Cheng, X Ai, and S C Lee. A mixed elastohydrodynamic lubrication model with asperity contact. *Journal of tribology*, 121(3):481–491, 1999.

[22] J Zhao, F Sadeghi, and M H Hoeprich. Analysis of ehl circular contact start up: Part imixed contact model with pressure and film thickness results. *Journal of tribology*, 123(1):67–74, 2001.

[23] Y Liu, Q J Wang, W Wang, Y Hu, and D Zhu. Effects of differential scheme and mesh density on ehl film thickness in point contacts. *Journal of Tribology*, 128(3):641–653, 2006.

[24] D Zhu. On some aspects of numerical solutions of thin-film and mixed elastohydrodynamic lubrication. *Proceedings of the Institution of Mechanical Engineers, Part J: Journal of Engineering Tribology*, 221(5):561–579, 2007.

[25] Y Liu, Q J Wang, D Zhu, WZ Wang, and Y Hu. Effects of differential scheme and viscosity model on rough-surface point-contact isothermal ehl. *Journal of Tribology*, 131(4):044501, 2009.

[26] WZ Wang, YZ Hu, YC Liu, and D Zhu. Solution agreement between dry contacts and lubrication system at ultra-low speed. *Proceedings of the Institution of Mechanical Engineers, Part J: Journal of Engineering Tribology*, 224(10):1049–1060, 2010.

[27] D Zhu, J Wang, N Ren, and Q J Wang. Mixed elastohydrodynamic lubrication in finite roller contacts involving realistic geometry and surface roughness. *Journal of Tribology*, 134(1):011504, 2012.

[28] W Pu, J Wang, Y Zhang, and D Zhu. A theoretical analysis of the mixed elastohydrodynamic lubrication in elliptical contacts with an arbitrary entrainment angle. *Journal of Tribology*, 136(4):041505, 2014.

[29] MJA Holmes, HP Evans, TG Hughes, and RW Snidle. Transient elastohydrodynamic point contact analysis using a new coupled differential deflection method part 1: theory and validation. *Proceedings of the Institution of Mechanical Engineers, Part J: Journal of Engineering Tribology*, 217(4):289–304, 2003.

[30] S Li and A Kahraman. A mixed ehl model with asymmetric integrated control volume discretization. *Tribology International*, 42(8):1163–1172, 2009.

[31] N Ren, D Zhu, WW Chen, and Q J Wang. Plasto-elastohydrodynamic lubrication (pehl) in point contacts. *Journal of tribology*, 132(3):031501, 2010.

[32] T He, J Wang, Z Wang, and D Zhu. Simulation of plasto-elastohydrodynamic lubrication in line contacts of infinite and finite length. *Journal of Tribology*, 137(4):041505, 2015.

[33] Q Dong and K Zhou. Numerical modeling of elastohydrodynamic lubrication in point or line contact for heterogeneous elasto-plastic materials. *Mechanics of Advanced Materials and Structures*, 24(15):1300–1308, 2017.

[34] M Renouf, F Massi, N Fillot, and A Saulot. Numerical tribology of a dry contact. *Tribology International*, 44(7-8):834–844, 2011.

[35] H Ghaednia, X Wang, S Saha, Y Xu, A Sharma, and R L Jackson. A review of elastic–plastic contact mechanics. *Applied Mechanics Reviews*, 69(6):060804, 2017.

[36] K L Johnson and Roberts A D Kendall, K. Surface energy and the contact of elastic solids. *Proc. R. Soc. Lond. A*, 324(1558):301–313, 1971.

[37] KNG Fuller and D Tabor. The effect of surface roughness on the adhesion of elastic solids. *Proc. R. Soc. Lond. A*, 345(1642):327–342, 1975.

[38] WR Chang, I Etsion, and D B Bogy. An elastic-plastic model for the contact of rough surfaces. *Journal of tribology*, 109(2):257–263, 1987.

[39] Y Zhao, D M Maietta, and L Chang. An asperity microcontact model incorporating the transition from elastic deformation to fully plastic flow. *Journal of Tribology*, 122(1):86–93, 2000.

[40] A Beheshti and MM Khonsari. Asperity micro-contact models as applied to the deformation of rough line contact. *Tribology International*, 52:61–74, 2012.

[41] L Kogut and I Etsion. Elastic-plastic contact analysis of a sphere and a rigid flat. *Journal of applied Mechanics*, 69(5):657–662, 2002.

[42] L Kogut and I Etsion. A finite element based elastic-plastic model for the contact of rough surfaces. *Tribology transactions*, 46(3):383–390, 2003.

[43] R L Jackson and I Green. A finite element study of elasto-plastic hemispherical contact against a rigid flat. *Journal of tribology*, 127(2):343–354, 2005.

[44] R L Jackson and I Green. A statistical model of elasto-plastic asperity contact between rough surfaces. *Tribology International*, 39(9):906–914, 2006.

[45] R L Jackson, H Ghaednia, and S Pope. A solution of rigid–perfectly plastic deep spherical indentation based on slip-line theory. *Tribology Letters*, 58(3):47, 2015.

[46] Tao He, N Ren, D Zhu, and J Wang. Plasto-elastohydrodynamic lubrication in point contacts for surfaces with three-dimensional sinusoidal waviness and real machined roughness. *Journal of Tribology*, 136(3):031504, 2014.

[47] G Xu, DA Nickel, F Sadeghi, and X Ai. Elastoplastohydrodynamic lubrication with dent effects. *Proceedings of the Institution of Mechanical Engineers, Part J: Journal of Engineering Tribology*, 210(4):233–245, 1996.

[48] N Rongjun H Ping. The influences of elastic-plastic deformation of rough surfaces on elastohydrodynamic lubrication for line contacts [j]. *Lubrication Engineering*, 6:005, 2006.

[49] N Ren, D Zhu, and Q J Wang. Three-dimensional plasto-elastohydrodynamic lubrication (pehl) for surfaces with irregularities. *Journal of Tribology*, 133(3):031502, 2011.

[50] C Jacq, D Nelias, G Lormand, and D Girodin. Development of a three-dimensional semi-analytical elastic-plastic contact code. *Journal of Tribology*, 124(4):653–667, 2002.

[51] W W Chen, L Shuangbiao, and Q J Wang. Fast fourier transform based numerical methods for elasto-plastic contacts of nominally flat surfaces. *Journal of applied mechanics*, 75(1), 2008.

[52] F Sahlin, R Larsson, A Almqvist, PM Lugt, and P Marklund. A mixed lubrication model incorporating measured surface topography. part 1: theory of flow factors. *Proceedings of the Institution of Mechanical Engineers, Part J: Journal of Engineering Tribology*, 224(4):335–351, 2010.

[53] X Ai. Numerical analyses of elastohydrodynamically lubricated line and point contacts with rough surfaces by using semi-system and multigrid methods (volumes 1 and 2). 1993.

[54] R Gohar. *Elastohydrodynamics*. World Scientific, 2001.

[55] S Liu, Q Wang, and G Liu. A versatile method of discrete convolution and fft (dc-fft) for contact analyses. *Wear*, 243(1):101–111, 2000.

[56] WZ Wang, H Wang, YC Liu, YZ Hu, and D Zhu. A comparative study of the methods for calculation of surface elastic deformation. *Proceedings of the Institution of Mechanical Engineers, Part J: Journal of Engineering Tribology*, 217(2):145–154, 2003.

[57] KL Johnson. Contact mechanics cambridge univ. *Press, Cambridge*, 1985.

[58] D Tabor. The hardness of materials. *Claredon Press, Oxford, UK*, 131:357–364, 1951.

[59] AL Ishlinsky. The problem of plasticity with axial symmetry and brinell's test. *Journal of Applied Mathematics and Mechanics*, pages 201–224, 1944.

[60] SS Wadwalkar, R L Jackson, and L Kogut. A study of the elasticplastic deformation of heavily deformed spherical contacts. *Proceedings of the Institution of Mechanical Engineers, Part J: Journal of Engineering Tribology*, 224(10):1091–1102, 2010.

[61] R L Jackson, I Green, and D B Marghitu. Predicting the coefficient of restitution of impacting elastic-perfectly plastic spheres. *Nonlinear Dynamics*, 60(3):217–229, 2010.

[62] S D Mesarovic and N A Fleck. Spherical indentation of elastic–plastic solids. In *Proceedings of the Royal Society of London A: Mathematical, Physical and Engineering Sciences*, volume 455, pages 2707–2728. The Royal Society, 1999.

[63] N Ye and K Komvopoulos. Indentation analysis of elastic-plastic homogeneous and layered media: Criteria for determining the real material hardness. *Journal of Tribology*, 125(4):685–691, 2003.

[64] L Kogut and K Komvopoulos. Analysis of the spherical indentation cycle for elastic–perfectly plastic solids. *Journal of materials research*, 19(12):3641–3653, 2004.

[65] J Alcalá and D Esqué-de los Ojos. Reassessing spherical indentation: Contact regimes and mechanical property extractions. *International Journal of solids and structures*, 47(20):2714–2732, 2010.

[66] W Yu and J.P. Blanchard. An elastic-plastic indentation model and its solutions. *Journal of materials research*, 11(9):2358–2367, 1996.

[67] YZ Hu and K Tonder. Simulation of 3-d random rough surface by 2-d digital filter and fourier analysis. *International journal of machine tools and manufacture*, 32(1-2):83–90, 1992.

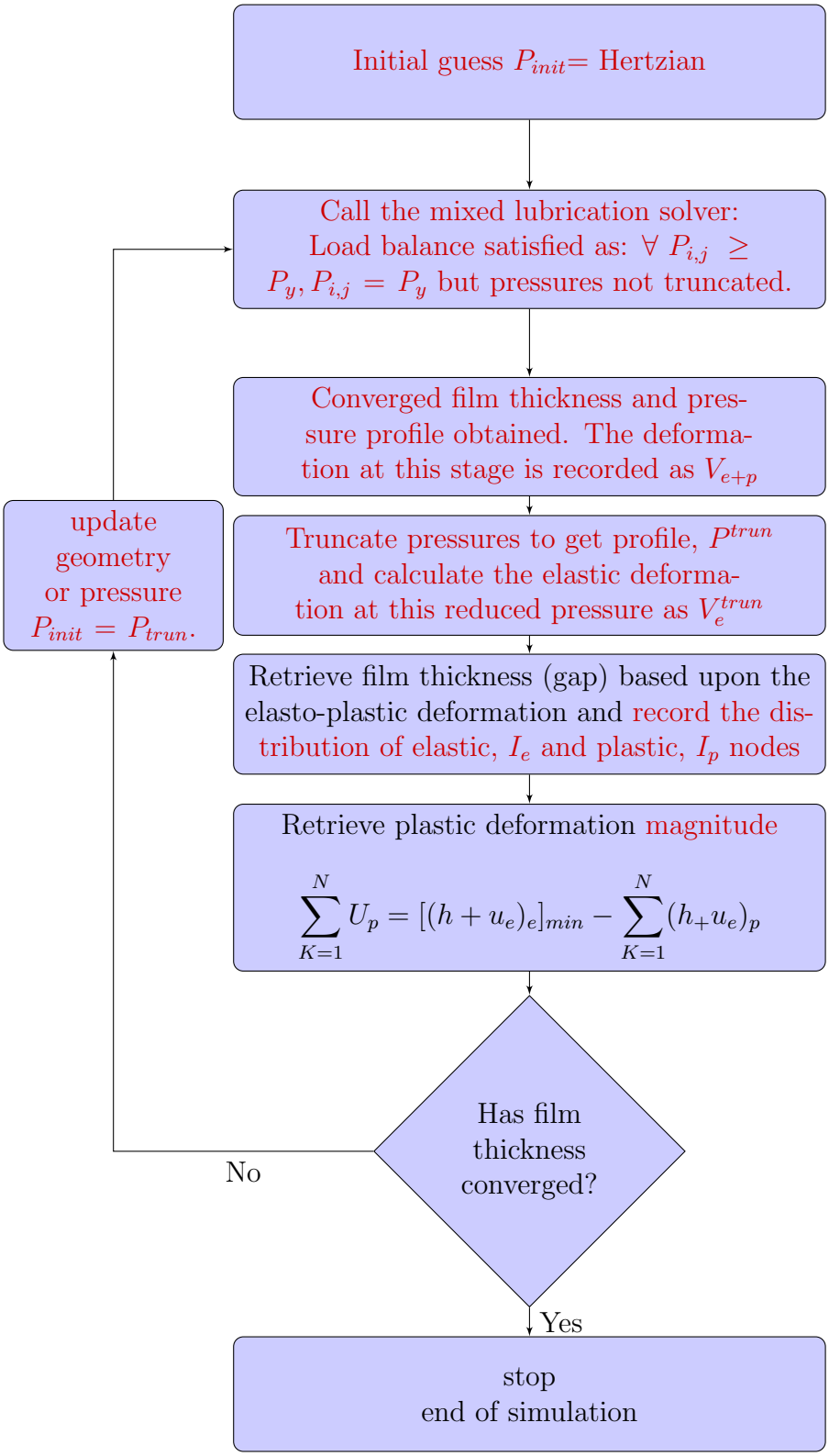


Figure 1: Flow chart to illustrate the PEHL model.

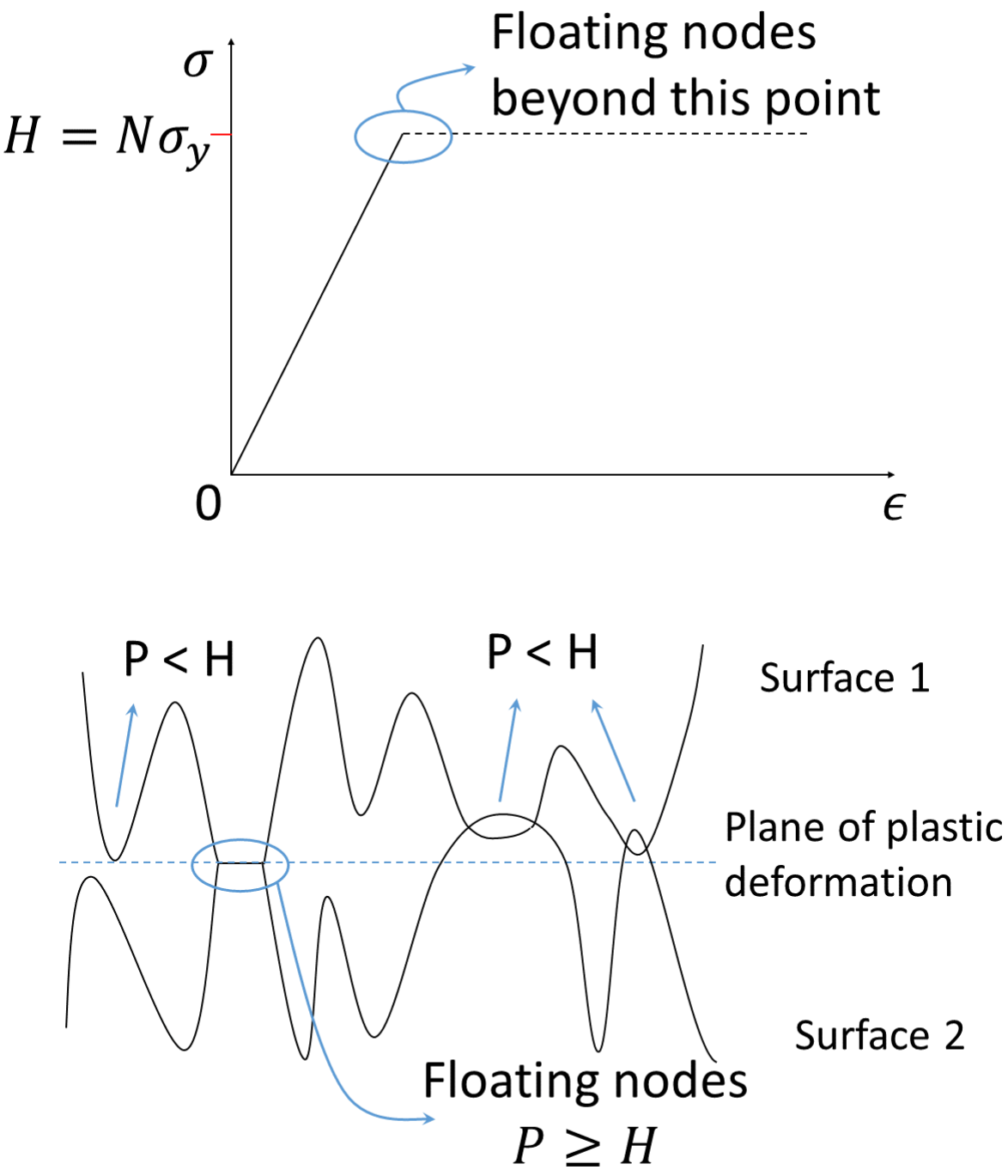


Figure 2: An illustration of the floating nodes in the PEHL solver. Top: the conceptual explaination of floating nodes. Bottom: geometrical explanation of floating nodes.

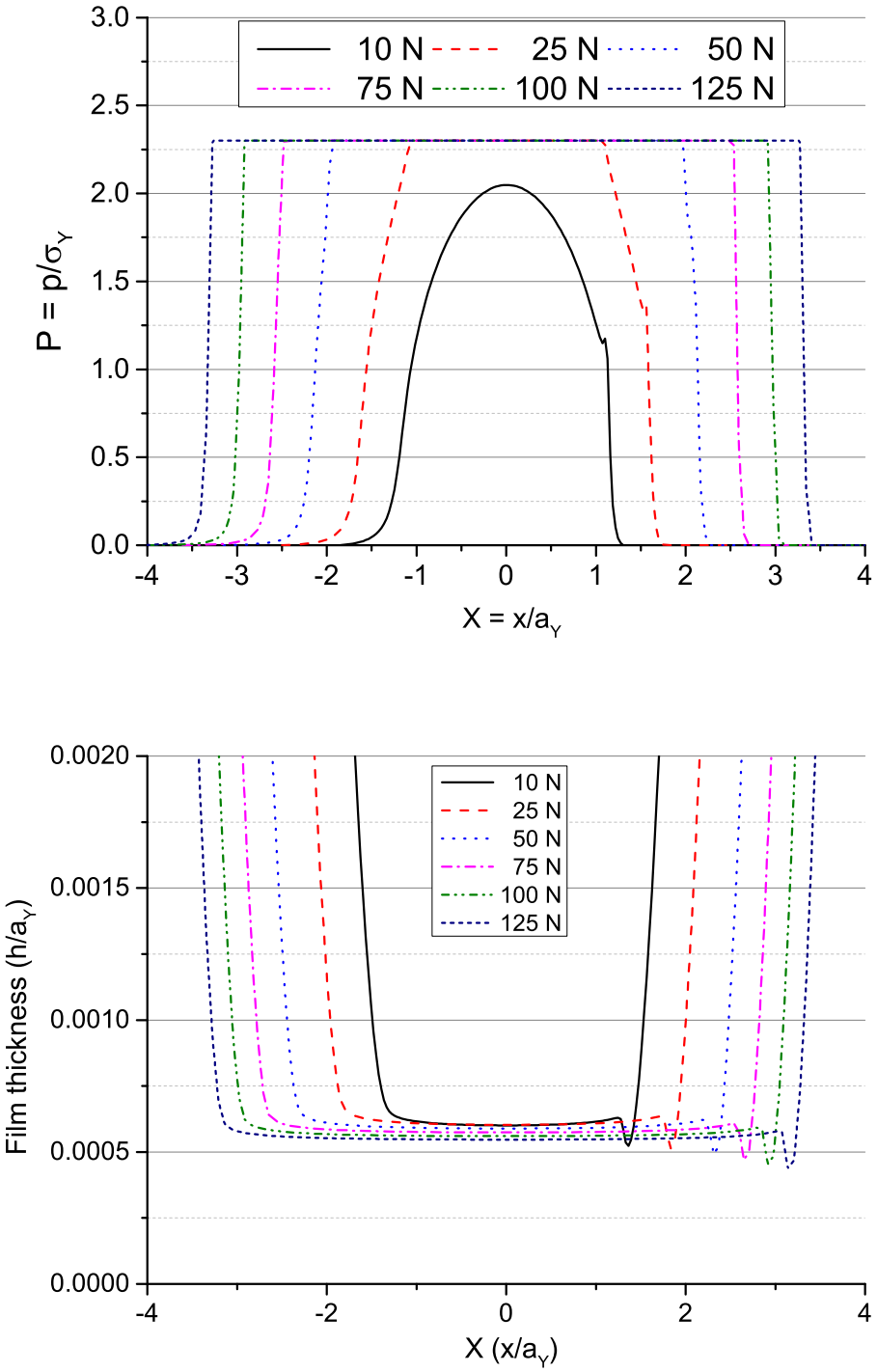


Figure 3: Contact characteristics for PEHL. (top) pressure profile, (bottom) film thickness profile. Six different force levels have been used as labelled.

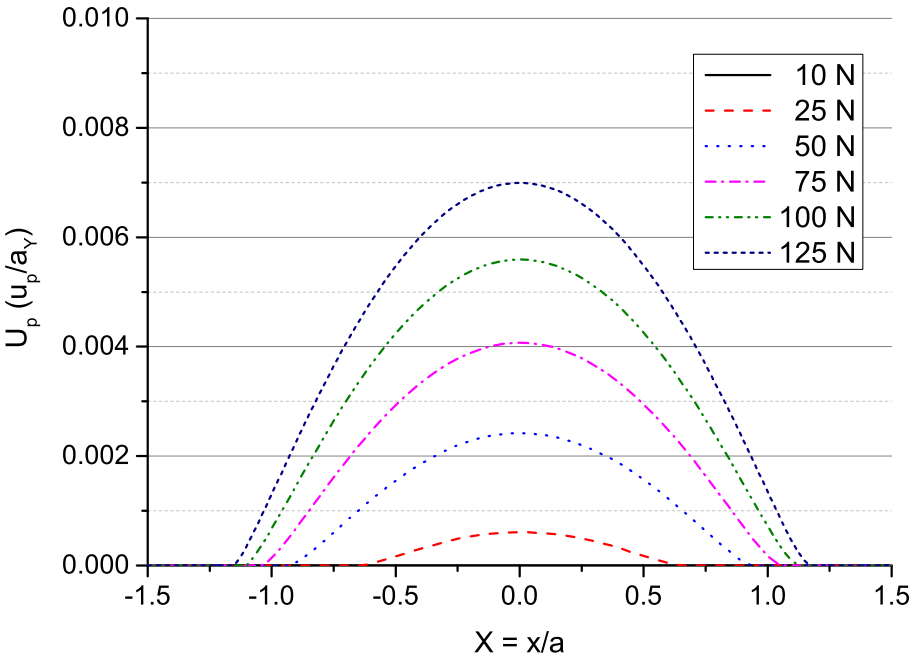


Figure 4: Variation of the magnitude of plastic deformation with load.

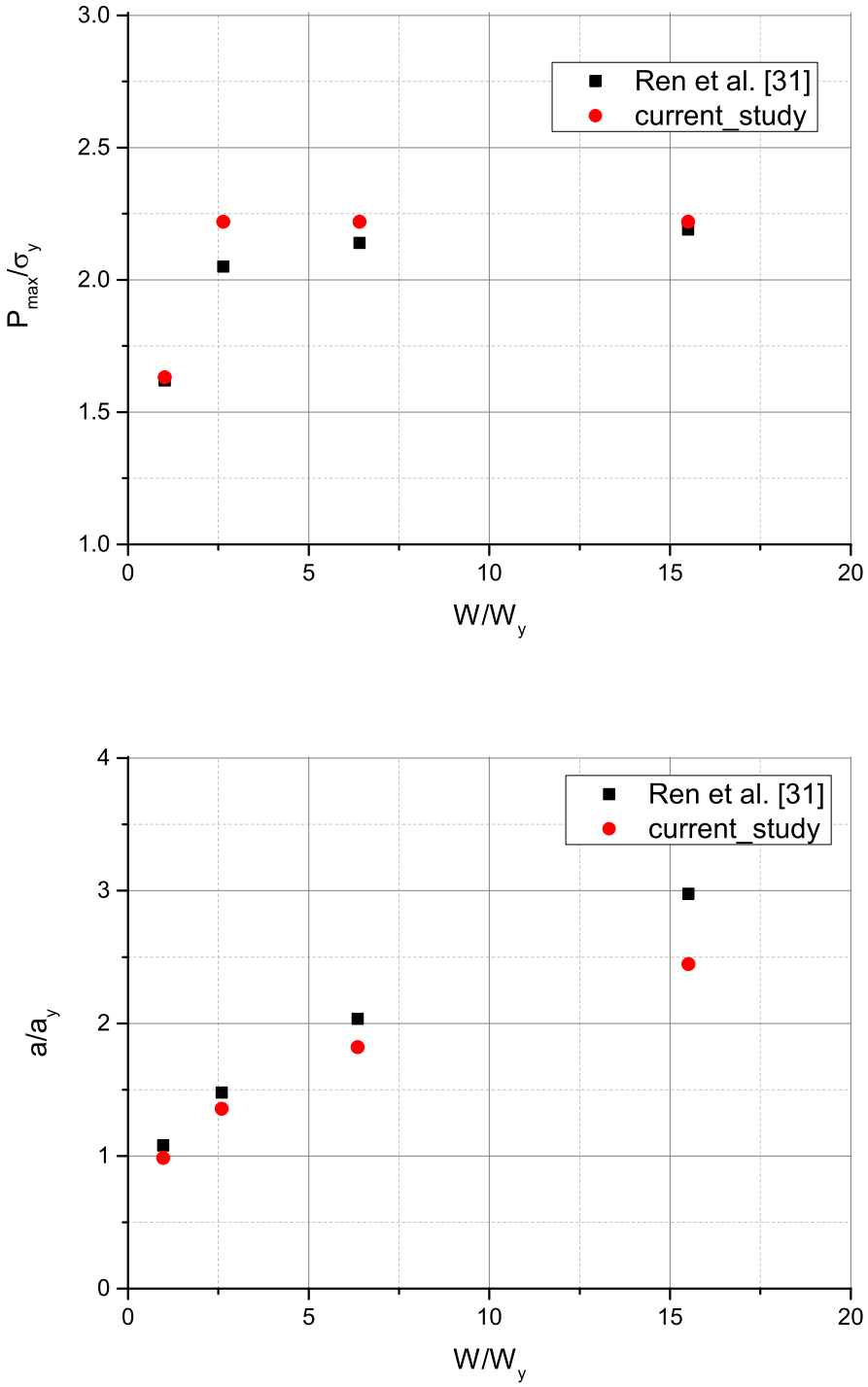


Figure 5: Comparison of PEHL results from current study and Ren et al. [31]

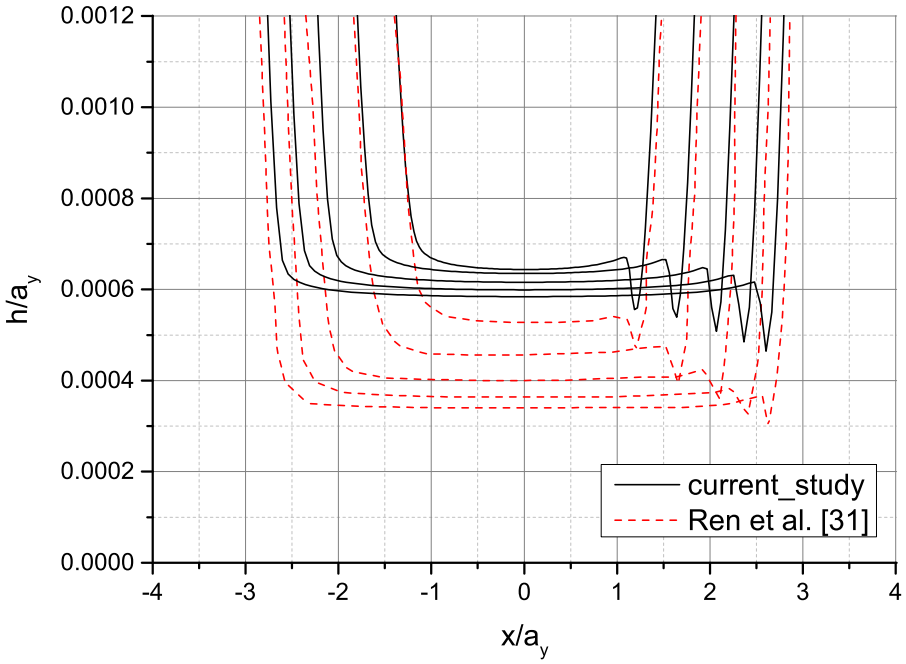


Figure 6: Comparison of EHL results from current study and Ren et al. [31]

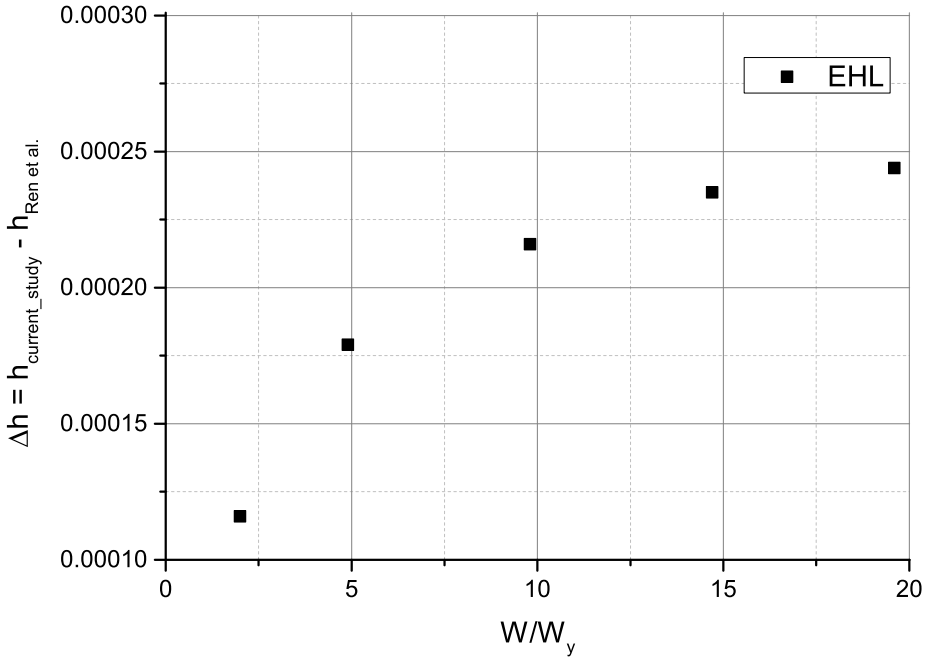


Figure 7: The difference in the predictions of film thickness results from current study and Ren et al. [31]

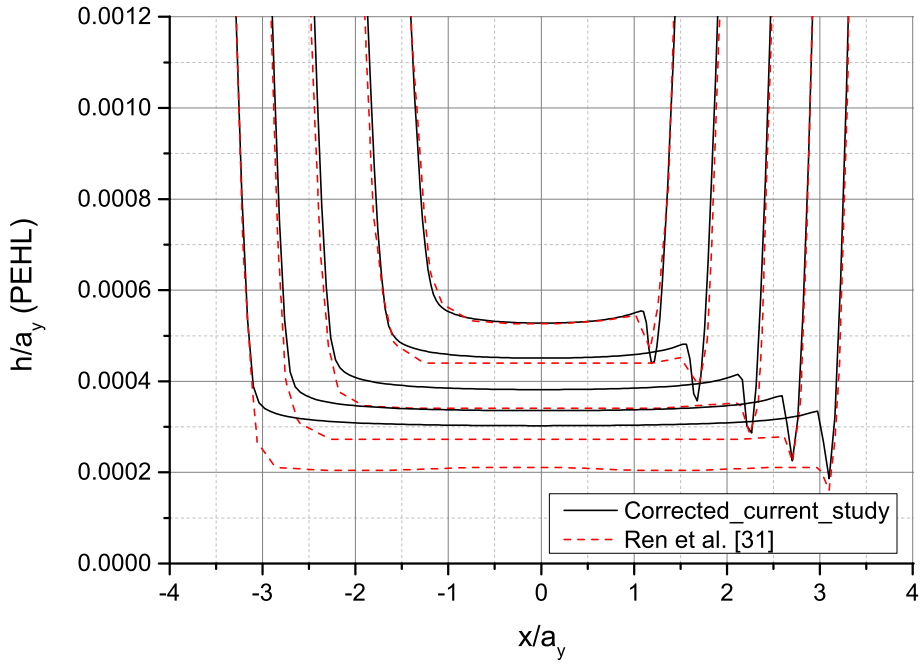


Figure 8: The corrected PEHL film thickness values.

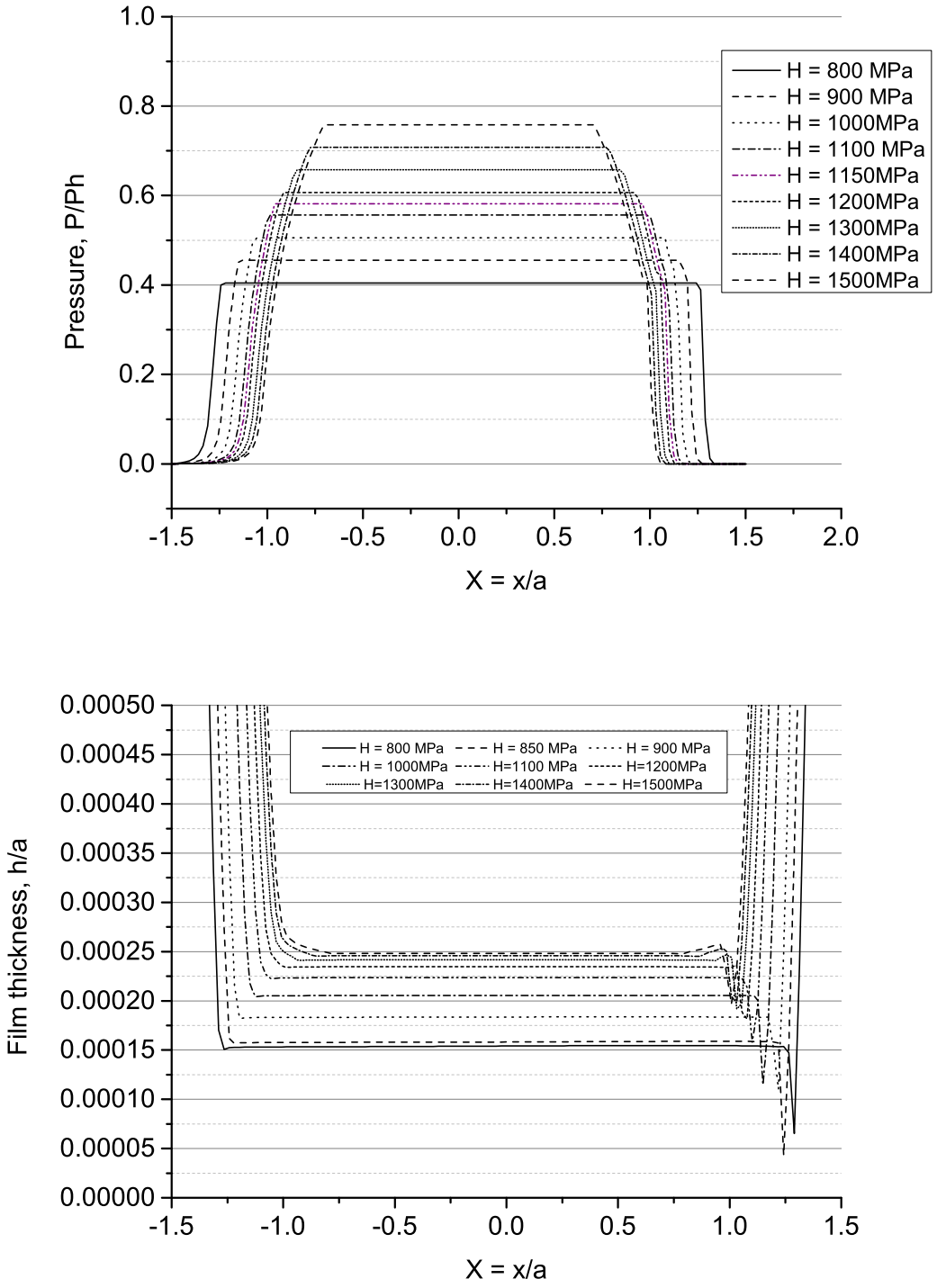


Figure 9: A comparison of the effect of the choice of hardness value on the PEHL characteristics. (top) Pressure profiles (bottom) film thickness profiles.

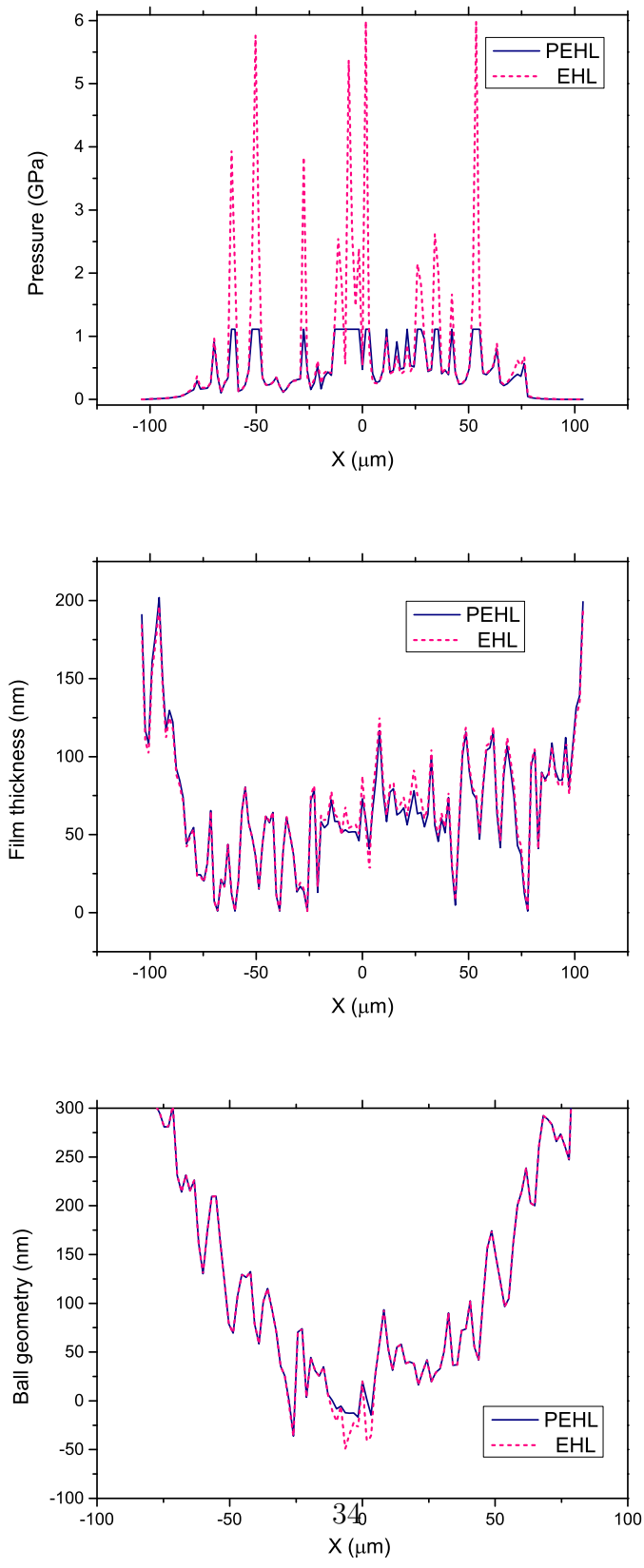




Figure 10: An illustration of the application of the PEHL model to rough surfaces. Top: pressure profile. Middle: film thickness profile. Bottom: permanently deformed ball geometry.